Usak University Journal of Material Sciences
journal homepage: http://uujms.usak.edu.tr

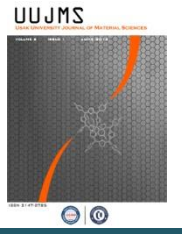

Research article

Finite element analysis of the thermo-mechanical behavior of the resistance spot welding

Murat Vural

Faculty of Mechanical Engineering, Istanbul Technical University, Istanbul, Turkey

Received 2 August 2012 *Revised 26 April 2013* *Accepted 17 June 2013*

Abstract

In this study, the formation of the welding nugget and the effect of welding process parameters on nugget shape and size, have been studied. And a combined thermal-electrical-mechanical simulation system is done using a Finite Element Analysis program, and the effect of the welding parameters such as current, time, electrode force, contact resistance temperature distribution on the contact resistance were investigated. The results provided useful information source on the formation of the nugget, and thus provided opportunities to play first true estimate of the quality of welding process.

©2013 Usak University all rights reserved.

Keywords: *Resistance spot welding, finite element analysis, welding nugget*

1. Introduction

In this study, the formation of the welding nugget and the effect of welding process parameters on nugget shape and size, have been studied. Finite element analysis was done to investigate the formation of a weld nugget of the resistance spot welding. A combined thermal-electrical-mechanical simulation system is done using a Finite Element Analysis program, and the effect of the welding parameters such as current, time, electrode force, contact resistance temperature distribution on the contact resistance were investigated. The aim of the study is to obtain an optimization for the resistance spot welding, using the results of this analysis.

In the electrical resistance spot welding process, the heat used for the welding is obtained from the electrical resistance of the material to the electric current passing through it. The heat occurs on the contact surface of two sheet material according to Joule Law.

$$Q = \eta\, I^2\, R\, T \tag{1}$$

where Q is the generated heat (J), η is a coefficient for the efficiency of the process, I is welding current (A), R is the sum of resistance in the circuit (Ω), and T is welding current duration in the circuit (s).

Corresponding author: Tel: +90–21 2–293 13 00/2500, Fax: +90–21 2–245 07 95
E-mail: vuralmu@itu.edu.tr
DOI: http://dx.doi.org/10.12748/uujms/20131710

©2013 Usak University all rights reserved.

The heat produced during the electric resistance spot welding is mainly used in the melting of the material locally. The material properties and characteristics of the environment causes an increase in the amount of heat needed because the heat is spread to the surrounding material and the environment. The heat distribution during welding is shown in Fig. 1. The heat transfer is a time-dependent function and the lost heat amount increases by time [1-3].

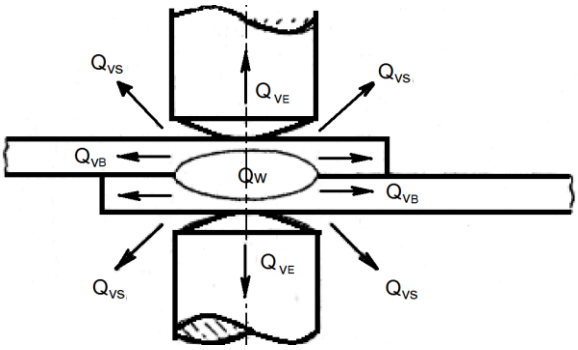

Fig. 1 Heat balance at the welding zone

$$\eta = \frac{Q_w}{Q_{zu}}\% \tag{2}$$

Related parameters in Eq. 2 could be calculated as below;

$$Q_w = Q_{zu} + Q_v \qquad Q_{zu} = c\int_{t=0}^{t=ts} l_s(t)R_s(t)dt \qquad Q_v = Q_{vE} + Q_{vB} + Q_{vS}$$

In these Eqs.; R_s is total resistance, Q_{zu} is the heat amount given to the weld nugget, t_s is welding time, Q_v is total heat amount lost, Q_{vE} is the heat amount conducted to the electrodes, Q_{VB} is the heat amount conducted to the surrounding material, Q_{vs} is the heat amount radiated to the surrounding environment and l_s is welding current.

All the parts of the electrical circuit can be seen as the resistance series which affect the flow of the current on the secondary circuit. Any amount of the heat produced on the resistances in this region will be proportional to the total amount of resistance. Therefore according to the principle of the method, the highest resistance in the weld zone and the minimum resistance level in other regions should be maintained. Fig. 2 shows the resistances on secondary circuit [4,5].

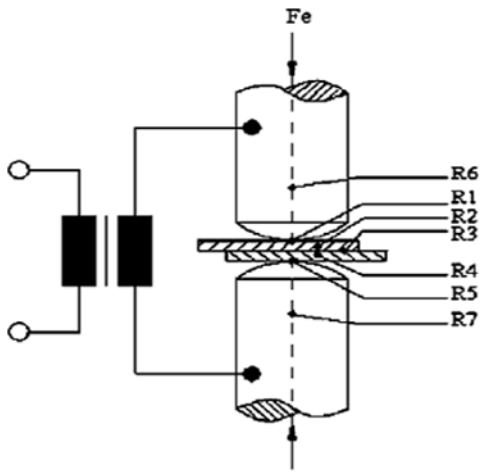

R_1, R_5 : Electrode- workpiece contact resistances; R_2, R_4:The bulk resistance of the workpieces; R_3:Workpiece-workpiece contact resistance; R_6, R_7:The bulk resistance of the electrodes; F_e: Electrode force

Fig. 2 The resistances at the weld zone

2. The Finite Element Analysis of the Formation of the Resistance Spot Weld Nugget

Compared to other methods, resistance spot welding process and the welding nugget analysis is harder because the melting and solidification processes events happen very quickly and also take place between the workpieces overlapped to each other [6]. This matter of general practice, the input data, for example the welding parameters, has been controlled to observe the final welding nugget. The input and output data cannot give satisfactory information about the formation and growing of the weld nugget. Therefore the complexity of the process increases even more, when considering the electrical, mechanical, thermal and metallurgical processes affecting to each other at the same time. Finite element method for such a matter appears to be a powerful tool to analyze the problem. The detailed temperature profile, stress and strain distribution, distortions in the different processes, can be defined by numerical methods. The effects of welding parameters, such as electrode force, electric current and the effects of stiffness of the welding power source, by changing the pre-simulation to investigate the effects of welding process. Experimental investigation of the effects of these process parameters is generally difficult [7,8].

While developing a finite element model, electrical, thermal and mechanical processes that can be formulated separately and then connected to each other process variables, must be considered on the basis of mutually dependent properties. On the other hand, these parameters are directly related with each other, so it would be more correct to consider the thermal and electrical processes at the same time. Coupling with the mechanical properties, it can be considered as the thermal effect of the stress-strain analysis. The main steps of electrical-thermal process can be classified as follows:

Firstly, the flow over the entire model as a proportioned amount of electrical voltage is obtained. Electric field, using the resistance of the material depending on the amount of energy released is calculated. Later, the energy has been using as a heat source and gained from electrical and thermal analysis, calculates the temperature distribution with

the help of heat conduction equation. All material properties is updated according to the temperature to be used stress-strain analysis. The surface of the electrode-sheet and sheet-sheet contact resistance has a very important role in this analysis. Physically, there is an acceptable artificial interface element which can be used for the simulation. This procedure and variable welding process parameters are (electrical current, contact resistance, electrical and thermal properties of the material and the electrode, and so on.) carried out to set up the simulation (Fig. 3).

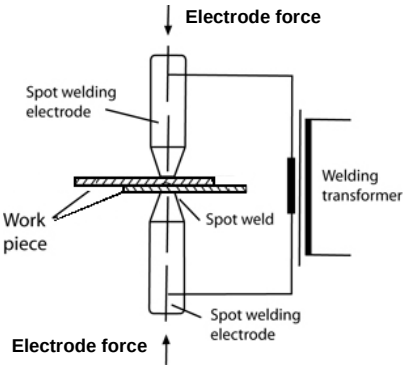

Fig. 3 Parameters affecting the resistance spot welding [9]

During the heating period, the material starts to melt, when it reaches to its melting point, and then allows to the formation of the weld nugget. It is generally hard to express mathematically a metallurgical melting phenomenon. The general practice to simulate melting phenomena is the sudden replacement of the property values of the material as modulus of elasticity, specific heat value and so on. Sudden increase in temperature of the specific heat with effect of hidden heat is expressed as follows:

$$\overline{C} = C + \frac{L}{T_L - T_S} \qquad (T_S<T<T_L) \tag{3}$$

Where L is latent heat, T_S is solidus temperature, T_L is liquidus temperature, C is specific heat of the material and $\overline{C}$ is sudden increase of the specific heat.

Solidification process can be viewed in the same way. Metal loses its ability to resist any load on the melting point. In a general practice, the temperature dependence of mechanical properties to create a just below the melting point of the value of modulus of elasticity to give low (about 10% less than the value at room temperature). Simulation in order to prevent convergence transition problems between values should be smooth. The concept of plastic deformation ends when it begins to melt, however this incident fails in the package simulation programs yet, special attention is required to show to solidified metal simulation [10,11].

3. Numerical Model

3.1. The Finite Elements Model

In this study, ANSYS finite element modeling program is used for simulation of the resistance spot welding. The model used has 6424 nodal points and 2190 elements (Fig.

4a). Representation of the model, applied loads and boundary conditions are shown in Fig. 4b.

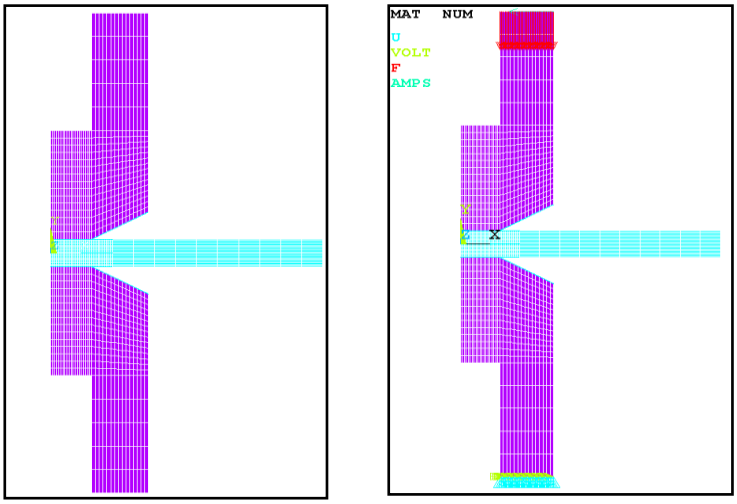

(a) (b)

Fig. 4 (a) Finite element model and (b) representation of the applied mechanical and electrical-thermal force

For the finite element model PLANE 223 type axisymmetric element was selected in the ANSYS 11.0 program. All equations in this study are based on two-dimensional cylindrical coordinate system [12].

Any correct definition of material properties and boundary conditions for numerical analysis is very important in terms of true-to-come of results. In Fig. 5, the electrical, mechanical and thermal boundary conditions are defined. A sinusoidal electrical current, with a frequency of 50 Hz, is properly distributed at the top surface of the upper electrode, and the flowing to the lower electrode (the point where the voltage value is zero) through the contact surfaces of respectively electrode-sheet, sheet-sheet arriving to the lower surface of lower electrode. In this state, the mean square root of the welding current (RMS) value can be written as:

$$I_{rms} = \sqrt{\frac{1}{\pi}\int_0^{\pi} (I_m \sin 2\pi ft)^2 d(2\pi ft)} = \frac{I_m}{\sqrt{2}} \tag{4}$$

In this equation: I_{rms}, represents welding current value, I_m, highest value of the current, I, real value of the current and f is frequency of the current as well.

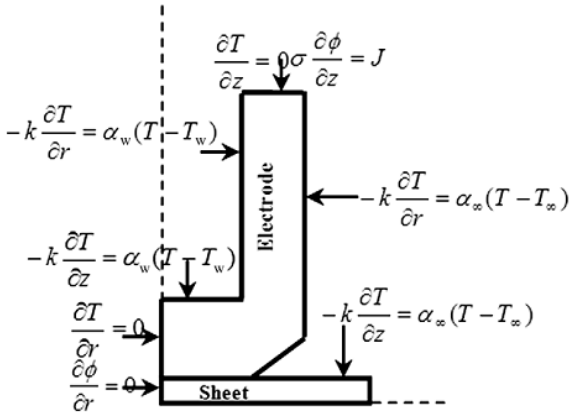

Fig. 5 Schematic representation of border conditions

Due to equation (3,4), the biggest current value is:

$$I_m = \sqrt{2} I_{rms} \tag{5}$$

Current value applied to the upper surface of the electrode is:

$$I = I_m \sin(2\pi ft) = \sqrt{2} I_{rms} \sin(2\pi ft) \tag{6}$$

For the lower side of the lower electrode, reference electrical voltage is defined as zero (*V=0*). To be able to represent the cooling of the electrodes inside surface, electrode-water contact surface temperature was accepted as constant and simulated. Also heat transfer coefficient 300 W/m^2.°C, and water temperature 25°C was accepted and modeled. Heat convection coefficient of the parts exposed to the atmosphere during the process was adopted as 21 W/m^2.°C and the reference temperature was accepted as 25 °C.

A force of 5000 N is applied during the solution process to each nodal point through Z axis on the upper side of the electrode. Because of choosing axially symmetric elements (axisymmetric), motion along the r axis, heat transfer and voltage drop was restricted. Therefore, it is not a necessary to define symmetry border conditions and degrees of freedom. For simplifying the analysis, slip on the electrode-sheet contact surface was neglected. For the solution of the model, electrical resistance welding process has been assumed as an electrical-thermal-structural problem, result was tried to obtain using the finite element solution with PLANE 223 type element. The model was solved in three load steps. In the first step, only compression is applied. Electrical, thermal or boundary conditions are not applied. In the second step, electrical, thermal and all structural forces are applied. The third step is the step in the structural and thermal loads are acting. Contact resistance, temperature-dependent material thermal, electrical and structural properties are taken into account during the solution change. Because of symmetric structure of electrode and work peace, axial symmetric elements are used and half of structure is modeled in 2D. In finite element model, there are three contact surfaces. The first and third contact surfaces are representing the surfaces of the electrode-sheet interface, while the second represents the surface of the contact surface of the sheet-

metal interface. To get close results to reality, fine mesh was formed near the contact surfaces and more coarse mesh was used for other parts (Fig. 6).

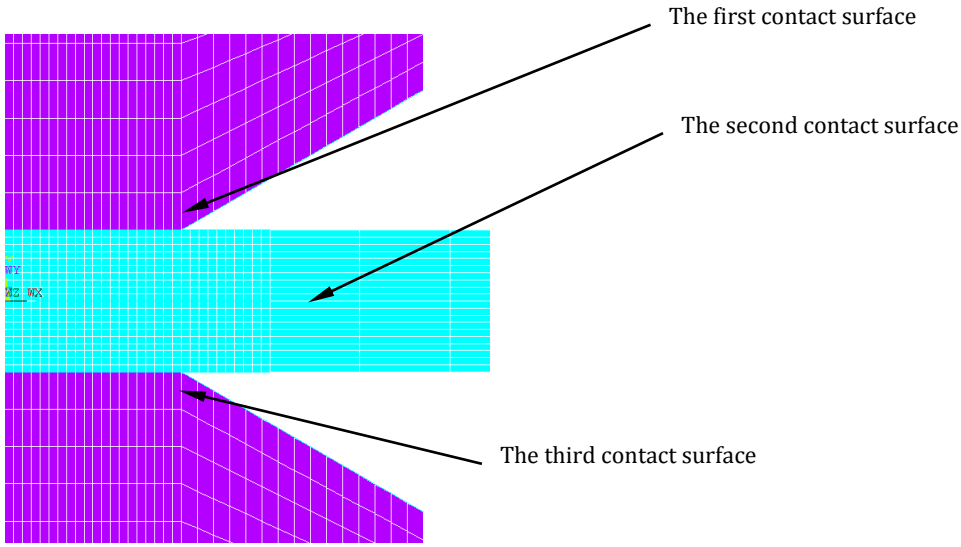

Fig. 6 The contact surfaces in the finite element model

The elements on the contact surface has also four degrees of freedom (DOF); UX, UY, TEMP, VOLT. Augmented Lagrangian was chosen as contact algorithm. The contact stiffness was updated after each iteration step,

3.2. Material Properties and Welding Parameters

Welding parameters used in this study is: Welding current: 14.2 kA; Welding period: 14 cycle (0.28 s); Electrode force: 5000 N; Compression time: 5 cycle (0.1 s)

Mechanical, thermal and electrical properties of materials used in the simulation model are given in Table 1 and Table 2. Because of the process characteristics, there is a large scale of temperature during process, so that material properties determined as temperature-dependent and used through this conception.

In this study, contact resistance is considered only temperature-dependent as a variable. In order to represent the value of the contact resistance between the model fields (electro-workpiece or sheet-metal contact surface) and ensure the transmission of electrical current depending on the temperature-ECR values are defined (Table 1). Contact surfaces of heat conduction were considered to be perfect; TEC value is defined as 5.0×10^{10}.

Table 1
The electrical and thermal properties of the materials used in the simulation model [13]

Temperature [°C]	Thermal Conductivity [W/m·°C]		Resistance [Ω.m]		Electrical Contact Resistance (ECR)		Specific Heat [J/kg·°C]	
	Steel	Copper	Steel	Copper	Sheet-sheet	Electrode-sheet	Steel	Copper
21	64.75	390.30	1.420×10^{-7}	2.640×10^{-8}	$8.40\times10^{+8}$	$7.09\times10^{+6}$	443.80	397.80
93	63.25	380.60	1.860×10^{-7}	3.000×10^{-8}	$8.66\times10^{+8}$	$7.46\times10^{+6}$	452.20	401.90
204	55.33	370.10	2.670×10^{-7}	4.000×10^{-8}	$8.89\times10^{+8}$	$7.73\times10^{+6}$	510.80	418.70
316	49.94	355.10	3.760×10^{-7}	5.050×10^{-8}	$9.43\times10^{+8}$	$8.32\times10^{+6}$	561.00	431.20
427	44.86	345.40	4.950×10^{-7}	6.190×10^{-8}	$1.04\times10^{+9}$	$9.21\times10^{+6}$	611.30	439.60
538	39.77	334.90	6.480×10^{-7}	6.990×10^{-8}	$1.12\times10^{+9}$	$1.01\times10^{+7}$	661.50	452.20
649	34.91	320.00	8.110×10^{-7}	8.000×10^{-8}	$1.53\times10^{+9}$	$1.39\times10^{+7}$	762.00	464.70
732							1004.00	
760	30.50	315.50	1.011×10^{-6}	8.980×10^{-8}	$3.53\times10^{+9}$	$3.24\times10^{+7}$	1004.00	477.30
774							1004.00	
799							1189.00	
871	28.41	310.30	1.115×10^{-6}	9.480×10^{-8}	$4.07\times10^{+9}$	$3.75\times10^{+7}$		
982	27.66	305.00	1.158×10^{-6}	9.980×10^{-8}	$4.80\times10^{+9}$	$4.42\times10^{+7}$		
1093	28.56	300.10	1.179×10^{-6}		$5.85\times10^{+9}$	$5.85\times10^{+7}$		
1204			1.209×10^{-6}				1189.00	502.40

For Steel: liquidus temp: 1521°C, solidus temp: 1482°C, latent heat: $2.72\text{x } 10^5$ J/kg

Table 2
The mechanical properties of the material used in the simulation model [14]

Temperature [°C]	Modulus of Elasticity [MPa]		Yield Strength [MPa]		Poisson Ratio		Thermal Expansion Coefficient (TEC) [1/°C]		Density [kg/m³]	
	Steel	Copper	Steel	Copper	Steel	Copper	Steel	Copper	Steel	Copper
21	206	124	248	83			1.098×10^{-5}	1.656×10^{-5}		
93	196	105	238	83			1.152×10^{-5}	1.674×10^{-5}		
204	194	93	224	83			1.224×10^{-5}	1.710×10^{-5}		
316	186	82	200	83			1.296×10^{-5}	1.746×10^{-5}		
427	169	55	172	83			1.350×10^{-5}	1.782×10^{-5}		
538	117	38	145	83			1.404×10^{-5}	1.836×10^{-5}		
649	55	25	76	83	0.30	0.32	1.458×10^{-5}	1.854×10^{-5}	7800	8900
732										
760		16					1.404×10^{-5}	1.890×10^{-5}		
774										
799										
871		14					1.350×10^{-5}	1.926×10^{-5}		
982		7								

4. Results and Discussion

Depending on the temperature distribution and time variation of the source region were obtained by simulation. In Fig. 7 the resulting temperature variation is observed during the welding process at the surface of the electrode-sheet and central part of the welding nugget (sheet-sheet contact interface). From the beginning of welding cycle, a rapid temperature rise within a very short period of time is observed. Material at the end of the first cycle approaches to a temperature of about 300°C (Fig. 8). The temperature increase on the surface of the electrode plate is slower. Due to contact resistance for surfaces, Joule warming is realized along the contact line. Because of the lower resistance between electrode-sheet contact surfaces, the temperature is relatively low. The highest temperature during the welding cycle absorbed at the center of contact surfaces of the workpieces. Therefore, the first melting takes place in this section, and then material dissolves close to this region. Thus, welding nugget can be obtained, as a result of melting material in a closed area.

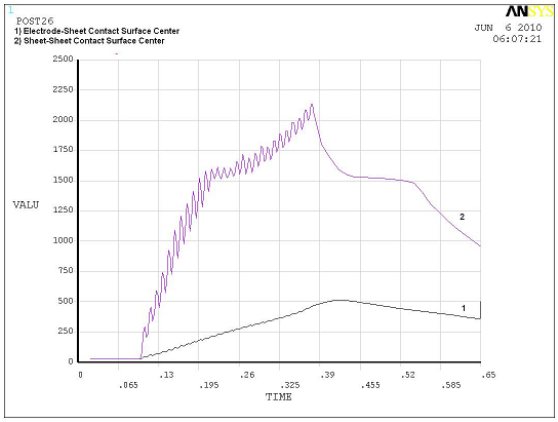

Fig. 7 Time-dependent temperature change at the surfaces of electrode-sheet and sheet-sheet

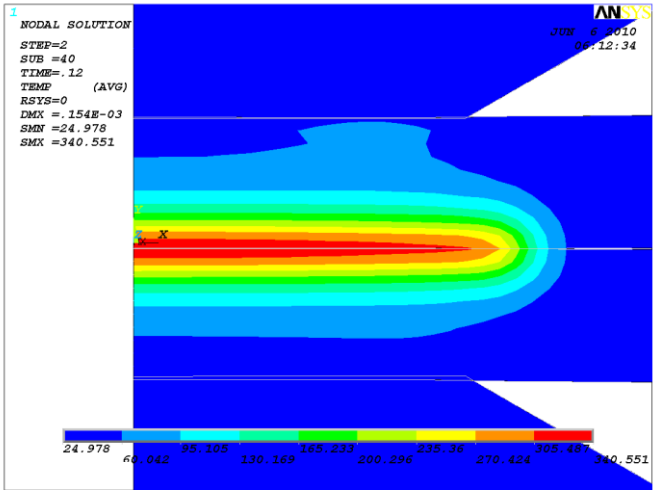

Fig. 8 Temperature distribution after first cycle

After the eighth cycle (~ 0.26 s), because of the highest temperature exceeds 1530°C, we accept that the material begins to melt (Fig. 9). This means the formation of nugget starts. The temperature distribution is almost in the form of a flat ellipse.

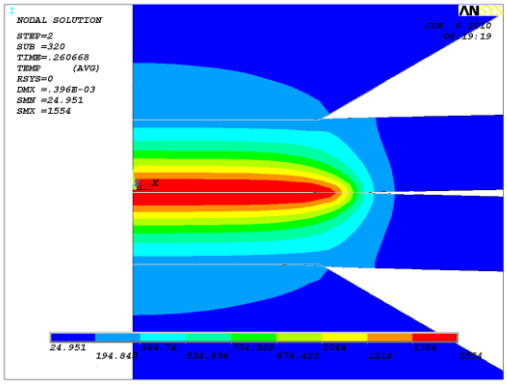

Fig. 9 Temperature distribution when the material reaches melting temperature

As the welding cycle goes on, current passes through material, temperature increases. Thus welding nugget continues growing. Highest temperature obtained in the nugget is, 2109°C. Fig. 10 shows the temperature distribution of highest values, Fig. 11 shows the HAZ and nugget form.

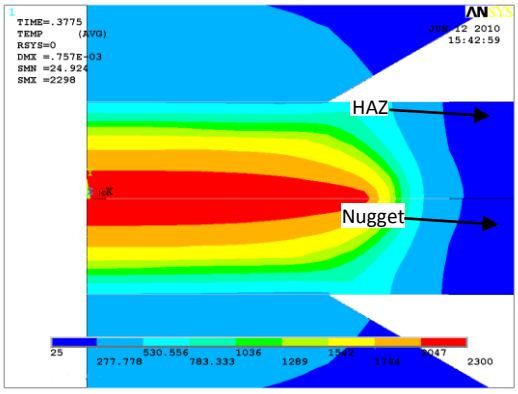

Fig. 10 Temperature distribution when material reaches highest temperature

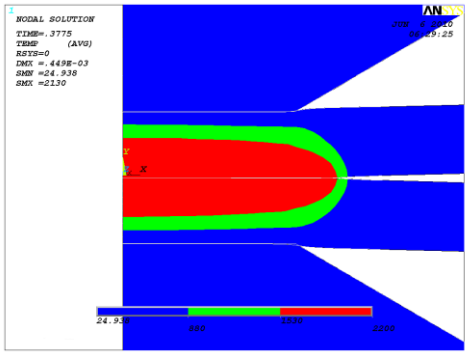

Fig. 11 The nugget and the HAZ geometry

After the reset cycle of electrical current from the source region begins to cool. In a very short period of time, temperature is decreased to 1500°C and it remains for a while at this temperature (latent heat) because of solidification (phase transformation). At the end of simulation (0.65 s) maximum temperature of nucleus falls below 1000°C. On the surface of the electrode-sheet intermediate temperature change rate (gradient) was lower than the surface of the sheet-metal intermediate. Electrode-sheet contact with the surface and the highest temperature are 0.38 s and 510°C, respectively.

With the same parameters used in the experimental study, with the core as a result of a study to compare the geometry of the core obtained by FEM is shown in Fig. 12. Nugget height is specified as 2.12 mm in the experimental study, FEM model, this value was calculated as 1.89. Comparison between the values when there is a difference of around 10%. This difference, the model used to say that it is possible to share a certain error.

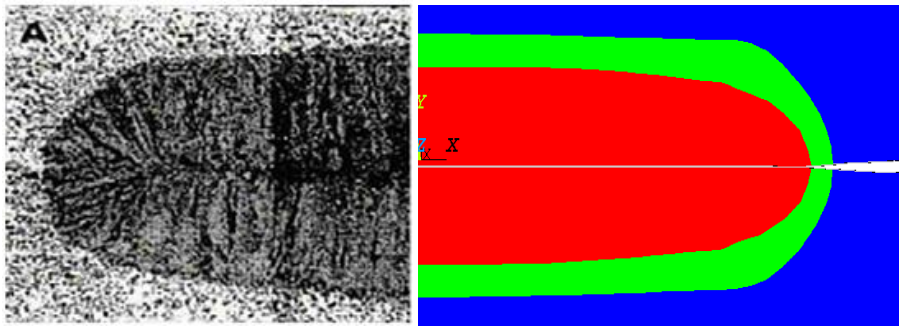

Fig. 12 Comparison of Nuggets with experimental study [2] and FEM analysis

In Fig. 13 temperature distribution for the given conditions are shown.

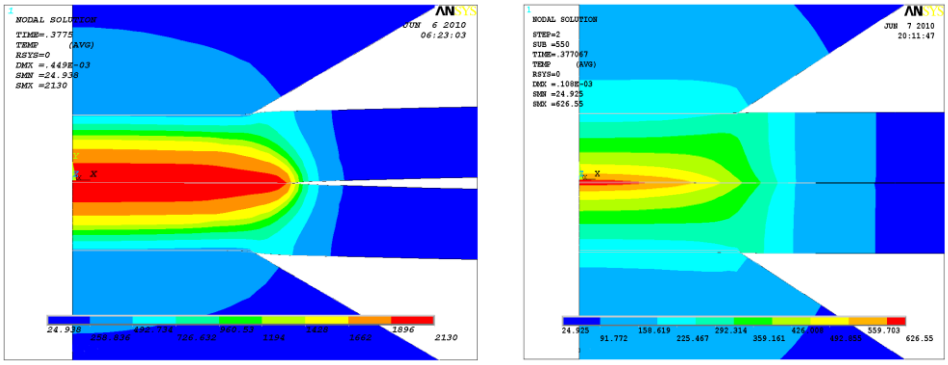

(a) Without shunt effect (b) With shunt effect

Fig. 13 Temperature distribution on the welding zone due to shunt effect

The increase in the force shape changes depending on the workpieces was also carried out a review of degrees of separation. Depending on the change of amount of separation and the rising of the high temperature values can be seen in Fig. 14. According to the results, opening between workpieces decreases with increasing the amount of force, that is, α angle decreases. Reason of the decreasing is, increasing of force causes to reduce contact resistance and consequently of this, high temperature value which is obtained using contact resistance decreases. As a consequence, because of reducing temperature zone and remaining high material stiffness value which remains high makes material shape changing difficult (Fig. 15).

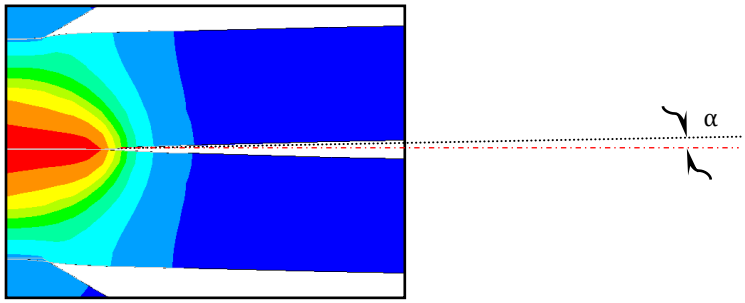

Fig. 14 Separation amount (angle) of the workpiece

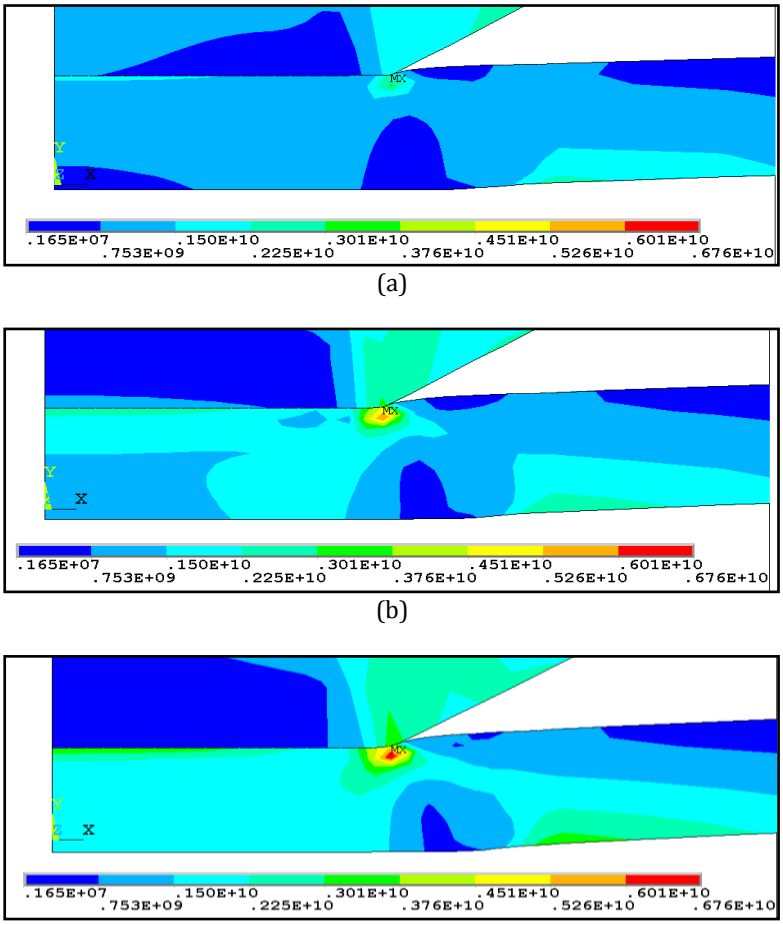

Fig. 15 Stress distribution for 14.2 kA welding current at highest temperature values (a) 3500 N, (b) 5000 N, and (c) 6000 N

5. Conclusions

This study using an electrical-thermal-structural finite element model aims to estimate the temperature distribution and nugget size of the resistance spot welding. Analogy to the provision of the required three combined analysis of the data and the type of boundary conditions, the source for the process to analyze the different phases were studied. At the same time, compliance with fair results for the control of an experimental study was based on the comparison with the results obtained. The results provided useful information source on the formation of the nugget, and thus opportunities to play first true estimate of the quality of welding process. Applied to the model input parameters can be achieved by editing the differences in the size of the welding nugget. As a result, to obtain desired quality and optimum values of workpieces with different materials, simulations can be used without large number of physical experiments.

References

1. Eisazadeh H, Hamedi M and Halvaee A. New parametric study of nugget size in resistance spot welding process using finite element method. Materials and Design Journal, 2009: 149 – 157.
2. Khan JA, Xu L, Chao Y and Broach K. Numerical simulation of resistance spot welding process. Numerical Heat Transfer, Part A, 2000; 37: 425 – 446.
3. Richard D, Fafard M, Lacroix R, Clery P and Maltais Y. Carbon to cast iron electrical contact resistance constitutive model for finite element analysis. Mater. Process Technology Journal, 2003; 132: 119 – 131.
4. Chang BH and Zhou Y. Numerical study on the effect of electrode force in small-scale resistance spot welding. Joining Material Process Technology, 2003; 139(1–3): 635 – 641.
5. Feulvarch E, Robin V and Bergheau JM. Resistance spot welding simulation: a general finite element formulation of electrothermal contact conditions. Joining Material Process Technology, 2004; 153: 436 – 441.
6. Feulvarch E, Robin V and Bergheau JM. Resistance spot welding process: experimental and numerical modeling of weld growth mechanisms with consideration of contact conditions. Numerical Heat Transfer Technology, Part A, 2006; 49: 345 – 367.
7. Hou Z and Kim I. Finite element analysis for the mechanical features of resistance spot welding process. Joining Material Process Technology, 2007; 180; 160 – 165.
8. Loulou T and Bardon JP. Estimation of thermal contact conductance during resistance spot welding. Exp Heat Transfer, 2001; 14: 251 – 264.
9. Loulou T and Bardon JP. Thermal characterization of resistance spot welding resistance spot welding. Numerical Heat Transfer, Part B, 2006; 49: 559 – 584.
10. Li BY and Lin ZQ. Numerical analysis of magnetic fluid dynamics behaviors during resistance spot welding. J Appl Phys, 2007; 101: 053506.
11. Babu SS, Santella ML, Feng Z, Riemer BW and Cohron JW. Empirical model of effects of pressure and temperature on electrical contact resistance of metals. Science and Technology of Welding and Joining, 2001; 6(3): 126 – 132.
12. ANSYS user manual
13. Vural M, Akkus A and Eryurek B. Effect of welding nugget diameter on the fatigue strength of the resistance spot welded joints of different steel sheets. Journal of Materials Processing Technology, 2006; 176: 127 – 132.
14. Vural M and Akkus A. On the resistance spot weldability of galvanized interstitial free steel sheets with austenitic stainless steel sheets. Journal of Materials Processing Technology, November 2004; Volumes 153-154: 1 – 6, 10.